Inorganic Chemistry

Article

pubs.acs.org/IC

5,10,15-Triferrocenylcorrole Complexes

Giuseppe Pomarico,[†] Pierluca Galloni,[†] Federica Mandoj,[†] Sara Nardis,[†] Manuela Stefanelli,[†] Andrea Vecchi,[†] Sara Lentini,[†] Daniel O. Cicero,[†] Yan Cui,[‡] Lihan Zeng,[‡] Karl M. Kadish,*[,‡] and Roberto Paolesse*[,†]

[†]Dipartimento di Scienze e Tecnologie Chimiche, Università di Roma Tor Vergata, via della Ricerca Scientifica 1, 00133 Rome, Italy

[‡]Department of Chemistry, University of Houston, Houston, Texas 77204-5003, United States

Supporting Information

ABSTRACT: Complexes of 5,10,15-triferrocenylcorrole were synthesized from the crude free-base corrole product obtained by the reaction of ferrocenyl aldehyde and pyrrole. Direct formation of the complex in this manner leads to an increase of the reaction yield by protecting the corrole ring toward oxidative decomposition. The procedure was successful and gave the expected product in the case of the copper and triphenylphosphinecobalt complexes, but an unexpected result was obtained in the case of the nickel derivative, where metal insertion led to a ring opening of the macrocycle at the 5 position, giving as a final product a linear tetrapyrrole nickel complex bearing two ferrocenyl groups. The purified 5,10,15-triferrocenylcorrole complexes have been fully characterized by a combination of spectroscopic methods, electrochemistry, spectroelectrochemistry, and density functional theory calculations. Copper derivatives of 10-monoferrocenyl- and 5,15-diferrocenylcorrole were prepared to investigate how the number and position of the ferrocenyl groups influenced the spectroscopic and electrochemical properties of the resulting complexes. A complete assignment of resonances in the ^{1}H and ^{13}C NMR spectra was performed for the cobalt and nickel complexes, and detailed electrochemical characterization was carried out to provide additional insight into the degree of communication between the *meso*-ferrocenyl groups on the conjugated macrocycle and the central metal ion of the ferrocenylcorrole derivatives.

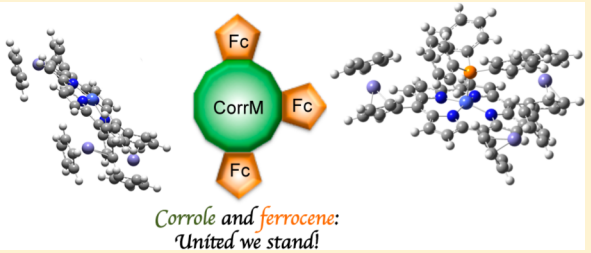

INTRODUCTION

Porphyrins and related macrocycles are a family of compounds widely distributed in biological systems, where they perform functions essential for life.[1] It is admirable how Nature is able to finely tune the reactions of these species by simple modifications in the molecular skeleton. For example, iron porphyrins are involved in oxygen activation and transport in animals, while magnesium chlorins are utilized in the photosynthetic processes of plants. These features have long attracted the interest of researchers, with one goal being the ability to use synthetic models that can imitate the chemistry of the natural systems while also allowing for the possibility of using these compounds in the development of new catalysts, electronic devices, drugs, and sensors.[2−7] Following the biological paradigm, a tuning of the metallomacrocycle properties can be carried out in different ways, starting from variation of the coordinated central metal ion to variation of the peripheral substituents and, finally, to changes in the molecular skeleton of the conjugated π-ring system.

Looking at these different approaches in the wide arena of different porphyrinoid structures, particular attention has been focused on ferrocene (Fc) as a peripheral substituent on the porphyrin ring.[8,9] One impetus for these synthetic studies has been the fact that Fc-containing porphyrins have shown, in the past, a specific redox activity with the possibility of obtaining compounds in mixed-valence states that can be exploited for optoelectronic applications.

From the point of view of porphyrin analogues, there has been a growing interest in corroles,[10,11] which are contracted porphyrins that show particular coordination and photophysical behavior and have promising applications in the areas of catalysis,[12−16] chemical sensors,[17] solar cells[18−20] and medicine.[21,22] Corroles act as trianionic ligands, which are characterized by a low oxidation potential and the ability to induce a facile ligand-to-metal electron transfer. These features lead corrole to generally behave as a noninnocent ligand.[23−25] Adding Fc as an electron-donor group at one or more meso positions of the corrole macrocycle should enhance the tendency of these compounds to undergo an oxidation process. Also, because one of the main features of Fc-based compounds is the formation of "mixed-valence state" derivatives,[26,27] the authors of this current manuscript wished to take advantage of these properties and have recently demonstrated the marriage of these two units with the preparation of a copper complex of 5,10,15-triferrocenylcorrole ($TFcCorrH_3$).[28]

We have now turned our attention to investigating how the number and positions of the *meso*-Fc groups on the corrole macrocycle will influence the physicochemical properties of the

Received: July 14, 2015
Published: October 13, 2015

DOI: 10.1021/acs.inorgchem.5b01575
Inorg. Chem. 2015, 54, 10256−10268

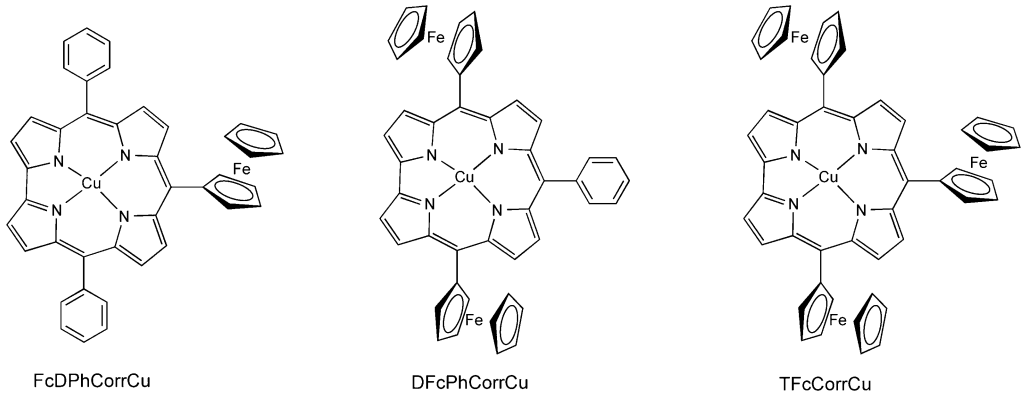

Figure 1. Molecular structures of copper corrolates bearing one, two, or three Fc groups.

compounds and report in the present paper a full characterization of the previously synthesized 5,10,15-triferrocenylcorrolatocopper(III) derivative, TFcCorrCu, together with the preparation and characterization of the corresponding mono- and bis-substituted Fc analogues, 5,15-diphenyl-10-ferrocenylcorrolatocopper(III) (FcDPhCorrCu) and 5,15-diferrocenyl-10-phenylcorrolatocopper(III) (DFcPhCorrCu), whose structures are shown in Figure 1.

Finally, we wished to explore the scope of the synthetic pathway leading to the ferrocenylcorrole complexes and examined the same procedures in an attempted synthesis of the cobalt and nickel triferrocenylcorrole derivatives. We were successful in the preparation and characterization of the corresponding triphenylphosphinecobalt(III) complex ($TFcCorrCoPPh_3$), but a nonoxidative ring opening of the $TFcCorrH_3$ macrocycle was observed during metalation with nickel acetate, giving as an isolated final product the linear diferrocenyltetrapyrrole derivative, DFcLTPNi, whose structure is shown in Figure 2. Both compounds were then characterized as to their spectroscopic and electrochemical properties.

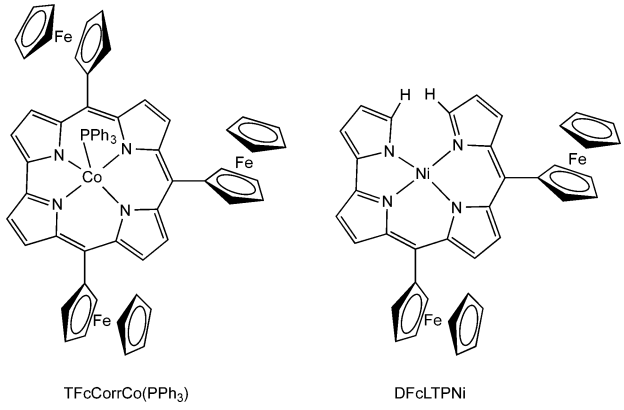

Figure 2. Molecular structures of the cobalt and nickel derivatives.

EXPERIMENTAL SECTION

General Procedures. Reagents and solvents (Sigma-Aldrich, Fluka, Merck, and Carlo Erba) were of synthetic grade and were used without further purification. Silica gel 60 (70−230 mesh) or neutral alumina (Brockmann grade III or IV) was used for chromatography. UV−visible spectra were measured in CH_2Cl_2 with a Varian Cary 50 spectrophotometer or a Hewlette-Packerd model 8453 diode-array spectrophotometer.

NMR Spectroscopy. ^1H and ^{13}C spectra were recorded at 300 K either with a Bruker AV300 spectrometer operating at 300 MHz or with a Bruker Avance 600 MHz spectrometer operating at 600 MHz for ^1H and 150 MHz for ^{13}C, equipped with a 5 mm inverse broadband probe and *z*-axis gradients. All experiments were performed in $CDCl_3$ at 300 K. Chemical shifts are given in ppm relative to a residual solvent (7.26 ppm for ^1H and 77.3 ppm for ^{13}C). NOESY spectra were acquired with a spectral window of 3.4 kHz (carrier frequency at 6.55 ppm) using 8192 t_2 data points (512 t_1 increments) and four transients with a relaxation delay of 2 s and a mixing time of 800 ms. COSY spectra were collected with a spectral window of 5.4 kHz (carrier frequency at 5 ppm) using 4096 t_2 data points (256 t_1 increments) and four transients with a relaxation delay of 2 s. $^1H-^{13}C$ HSQC experiments were acquired with a spectral window of 13.6 kHz and a carrier frequency at 45 ppm (aliphatic region) or a spectral window of 9 kHz and a carrier frequency at 120 ppm (aromatic region) using 4096 t_2 data points (256 t_1 increments) and four transients with a relaxation delay of 2 s. $^1H-^{13}C$ HMBC experiments were acquired with a spectral window of 30 kHz (carrier frequency at 100 ppm) using 4096 t_2 data points (1024 t_1 increments) and 16 transients with a relaxation delay of 2 s. All data were processed with *TopSpin*.

Electrochemistry. Cyclic voltammetry was carried out with an EG&G model 173 potentiostat/galvanostat. A homemade three-electrode electrochemistry cell was used, which consisted of a platinum or glassy carbon working electrode, a platinum wire counter electrode, and a saturated calomel reference electrode (SCE). The SCE was separated from the bulk of the solution by a fritted-glass bridge of low porosity, which contained a solvent/supporting electrolyte mixture. All potentials are referenced to the SCE.

Thin-layer UV−visible spectroelectrochemical experiments were performed with a home-built thin-layer cell, which has a light-transparent platinum net working electrode. Potentials were applied and monitored with an EG&G PAR model 173 potentiostat. Time-resolved UV−visible spectra were recorded with a Hewlett-Packard model 8453 diode-array spectrophotometer. High-purity N_2 from Trigas was used to deoxygenate the solution and kept over the solution during each electrochemical and spectroelectrochemical experiment.

Synthesis. $TFcCorrH_3$ and TFcCorrCu were prepared as previously reported,[28] starting from ferrocenecarboxaldehyde (400 mg, 1.87 mmol) and pyrrole (0.65 mL, 9.35 mmol). $TFcCorrH_3$ was partially purified by an alumina oxide (grade IV) plug eluted with $CHCl_3$ to remove the polypyrrolic impurities before the reactions to insert the metal ions. Yields for the cobalt and nickel derivatives were calculated with respect the amount of ferrocenecarboxaldehyde used for the free-base corrole preparation.

(10-Ferrocenyl-5,15-diphenylcorrolato)copper (FcDPhCorrCu). 5-Phenyldipyrromethane[29] (400 mg, 1.80 mmol) and ferrocenecarboxaldehyde (192 mg, 0.90 mmol) were dissolved in 72 mL of methanol, after which 72 mL of aqueous HCl (0.6 M) was added to the solution and the mixture stirred at room temperature for 3 h. The suspension was extracted with $CHCl_3$, washed twice with water, dried

DOI: 10.1021/acs.inorgchem.5b01575
Inorg. Chem. 2015, 54, 10256−10268

over Na_2SO_4, and diluted with $CHCl_3$ to a volume of 270 mL, and 333 mg of chloranil (1.35 mmol) was added. This solution was stirred at room temperature for 15 min, after which a methanolic solution of $Cu(AcO)_2$ was added and the mixture stirred to reflux for 20 min. The solvent was removed and the mixture purified by a silica gel plug eluted with $CHCl_3$ to remove the decomposed material. Fractions containing the corrole were collected and purified again by column chromatography (silica gel and 1:1 CH_2Cl_2/hexane). The first eluted band corresponds to 5,10,15-triphenylcorrrolatocopper (TPCorrCu), followed by traces of copper porphyrin and then by the desired FcDPhCorrCu, which was crystallized with CH_2Cl_2/CH_3OH. Yield: 19 mg (3%). Mp: >300 °C. UV−vis [CH_2Cl_2; λ_{max}, nm (log ε, M^{-1} cm^{-1})]: 415 (5.01), 527 sh, 634 (3.90). ^{1}H NMR (300 MHz, $CDCl_3$): δ 8.49 (d, 2 H, J = 4.25 Hz, β-pyrrole), 7.90 (d, 2 H, J = 3.00, Hz, β-pyrrole), 7.82 (d, 4 H, J = 7.35 Hz, phenyls), 7.68 (d, 2 H, J = 4.05 Hz, β-pyrrole), 7.61 (d, 2 H, J = 6.93 Hz, phenyls), 7.56−7.51 (m, 4 H, phenyls), 7.47 (d, 2 H, J = 4.23 Hz, β-pyrrole), 5.04 (br s, 2 H, α-Cp), 4.68 (br s, 2 H, β-Cp), 4.23 (s, 5 H, CpH). MS (FAB): m/z 696 (100%). Elem anal. Calcd for $C_{41}H_{27}CuFeN_4$: C, 70.85; H, 3.91; N, 8.06. Found: C, 70.79; H, 3.85; N, 8.01.

(5,15-Diferrocenyl-10-phenylcorrolato)copper (DFcPhCorrCu). Ferrocenyldipyrromethane[30] (330 mg, 1.00 mmol) and benzaldehyde (51 μL, 0.50 mmol) were dissolved in 100 mL of methanol, and then 50 mL of aqueous HCl (0.6 M) was added and the mixture stirred at room temperature for 3 h. The suspension was extracted with $CHCl_3$, washed twice with water, dried over Na_2SO_4, and diluted with $CHCl_3$ to a volume of 250 mL, and 369 mg of chloranil (1.50 mmol) was added. The solution was stirred at room temperature for 15 min, after which a methanolic solution of $Cu(AcO)_2$ was added and the mixture further stirred to reflux for 20 min. The solvent was removed and the mixture purified by a silica gel plug eluted with $CHCl_3$ to remove any decomposed material. Fractions containing corrole were collected and purified again by column chromatography (silica gel and 3:2 CH_2Cl_2/hexane). The first eluted band corresponds to TFcCorrCu, followed by traces of copper porphyrin and then the desired DFcPhCorrCu, which was crystallized with CH_2Cl_2/CH_3OH. Yield: 8 mg (2%). Mp: >300 °C. UV−vis [CH_2Cl_2; λ_{max}, nm (log ε, M^{-1} cm^{-1})]: 420 (4.83), 666 (4.11). ^{1}H NMR (300 MHz, $CDCl_3$): δ 8.65 (d, 2 H, J = 3.90 Hz, β-pyrrole), 8.36 (br s, 2 H, β-pyrrole), 8.02 (br s, 2 H, β-pyrrole), 7.73 (d, 2 H, J = 7.62 Hz, phenyls), 7.62−7.50 (m, 3 H, phenyls), 7.36 (d, 2 H, J = 4.38 Hz, β-pyrrole), 5.07 (br s, 4 H, α-Cp), 4.66 (br s, 4 H, β-Cp), 4.22 (br s, 10 H, CpH). MS (FAB): m/z 805 (100%) Elem anal. Calcd for $C_{45}H_{31}CuFe_2N_4$: C, 67.31; H, 3.89; N, 6.98. Found: C, 67.22; H, 3.91; N, 6.93.

(Triphenylphosphine)(5,10,15-triferrocenylcorrolato)cobalt (TFcCorrCoPPh$_3$). The mixture containing $TFcCorrH_3$ was dissolved in $CHCl_3$ and CH_3OH (20 + 5 mL), and $Co(AcO)_2{\cdot}4H_2O$ (25 mg, 0.1 mmol) and PPh_3 (26 mg, 0.1 mmol) were added to solution. The mixture was refluxed for 20 min, while monitoring the course of the reaction by thin-layer chromatography (TLC; silica gel/CH_2Cl_2) and UV−visible spectroscopy. When the reaction was complete, following the disappearance of the starting material as determined by TLC, the solvent was removed under vacuum and the residue purified by a silica gel plug eluted with CH_2Cl_2. Fractions containing cobalt corrole were collected and purified again by a neutral Al_2O_3 plug eluted with 2:1 CH_2Cl_2/hexane. The green fraction, corresponding to TFcCorrCoPPh$_3$, was crystallized by CH_2Cl_2/CH_3OH. Yield: 22 mg (3%). Mp: >300 °C. UV−vis [CH_2Cl_2; λ_{max}, nm (log ε, M^{-1} cm^{-1})]: 405 (4.61), 598 (4.19). MS (FAB): m/z 904.6 (100%; M − PPh_3). Elem anal. Calcd for $C_{67}H_{50}CoFe_3N_4P$: C, 68.86; H, 4.31; N, 4.79. Found: C, 68.73; H, 4.11; N, 4.63.

Synthesis of a Nickel Complex. The mixture containing $TFcCorrH_3$ was dissolved in *N*,*N*-dimethylformamide (DMF; 8 mL), and $Ni(AcO)_2{\cdot}4H_2O$ (25 mg, 0.1 mmol) was added. The mixture was stirred at 80 °C for 10 min, while monitoring the course of the reaction by TLC (silica gel/CH_2Cl_2) and UV−visible spectroscopy. After the disappearance of the starting material on a TLC plate, water was added and the precipitate filtered. The residue was dissolved in $CHCl_3$, dried over Na_2SO_4, and purified on a silica gel column eluted with 1:1 CH_2Cl_2/hexane. A green fraction corresponding to the title compound was crystallized by CH_2Cl_2/CH_3OH. Yield: 9 mg (2%). Mp: >300 °C. UV−vis [CH_2Cl_2; λ_{max}, nm (log ε, M^{-1} cm^{-1})]: 401 sh, 456 (4.48), 659 (4.03), 740 (sh), 818 (3.98), 900 (4.02). MS (FAB): m/z 711.05. Elem anal. Calcd for $C_{38}H_{28}Fe_2N_4Ni$: C, 64.19: H, 3.97; N, 7.88. Found: C, 63.93; H, 3.91; N, 7.91.

Calculation Details. Computational calculations were performed using *Gaussian 09*, revision A.02.[31] Molecular orbitals (MOs) were visualized using *GaussView 5*. Geometry optimizations were performed with pure (BP86 and OLYP), pure meta (TPSSTPSS), and hybrid (B3LYP and CAM-B3LYP) generalized gradient approximation (GGA) functionals using a 6-31g(d,p) basis set.

RESULTS AND DISCUSSION

$TFcCorrH_3$ was prepared by the reaction of pyrrole with ferrocenyl aldehyde; this synthesis was carried out via two routes: one a modified Lindsey approach optimized in our laboratories for corrole synthesis[32] and the other a water/methanol route reported by Koszarna and Gryko.[33] The yields via these two approaches were generally comparable, and in both cases, formation of the desired free-base triferrocenylcorrole was accompanied by the corresponding free-base tetraferrocenylporphyrin, usually in lower amounts when following Koszarna and Gryko's method. A key factor strongly influencing the overall yield of $TFcCorrH_3$ was, however, facile oxidation of the macrocycle because, in addition to decomposition products, both isocorrole species and open-chain derivatives were observed in the reaction mixture. With the aim of limiting this drawback, we modified the synthetic protocol by adding copper acetate immediately after the oxidation step. Insertion of the metal ion, with formation of the copper complex, led to increased stability and reduced overoxidation that affected the free-base corrole. Although this modification does not allow one to directly obtain free-base corrole, the possibility to demetallate the copper complexes enables the preparation of free-base $TFcCorrH_3$ and metal derivatives upon treatment with the appropriate metal salt.

Spectroscopic characterization of TFcCorrCu indicated some interesting optical properties of this complex. Copper 5,10,15-triarylcorrolates exhibit UV−visible spectra that are strongly influenced by substituents at the *meso*-phenyl rings of the corrole and less affected by changes in substituents at the β-pyrrolic positions on the macrocycle.[34−38] Electron-donating groups induce significant red shifts in the Soret band, and this effect has been attributed to a phenyl (macrocycle)-to-metal ($3d_{x^2-y^2}$) charge-transfer character of the main absorbance band, inducing a 10−11% ligand-to-metal charge-transfer character for the B band.[38] This feature provides further evidence for the difficulty in characterizing electronic structures of such noninnocent ligands. This phenyl (macrocycle)-to-metal charge transfer also induces a saddlelike distortion of the tetrapyrrole ring,[39] even in the absence of peripheral substituent crowding, a unique case among all of the metallocorrolates.

On the other hand, the observed spectrum of TFcCorrCu (solid line in Figure 3) is quite different from spectra of the copper triarylcorrole complexes (see, for example, the TPCorrCu spectrum in Figure 3) and closely resembles that of the corresponding copper tetraferrocenylporphyrin complex.[30] For this latter corrole, it has been reported that the UV−visible spectroscopic pattern of the metalated macrocycle is predominantly influenced by Fc-based orbitals lying in energy between the occupied and unoccupied porphyrin-based orbitals.[30] For the corrole complexes, the situation is even more complicated because it has been reported in the literature

DOI: 10.1021/acs.inorgchem.5b01575
Inorg. Chem. 2015, 54, 10256−10268

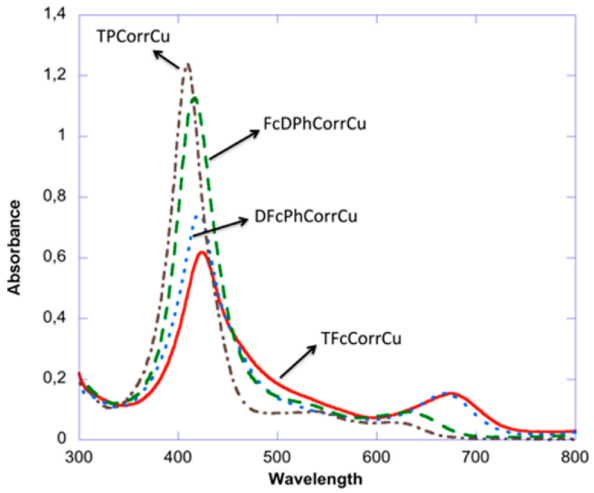

Figure 3. UV−visible spectra (10^{-5} M in CH_2Cl_2) of TFcCorrCu (solid line), DFcPhCorrCu (dotted line), FcDPhCorrCu (dashed line), and TPCorrCu (dash-dotted line).

that substituents at the meso positions 5 and 15 of the macrocycle contribute more to variations of the corrole UV−visible spectra than do substituents at the meso position 10.[36] To verify whether this feature is observed in the case of Fc-substituted corroles, copper derivatives were prepared with corroles bearing one, two, or three meso-substituted Fc groups (see the structures in Figure 1). FcDPhCorrCu and DFcPhCorrCu were prepared following a method reported for the synthesis of trans A_2B corroles, starting from the appropriate dipyrromethane and aldehyde.[33] As was done for TFcCorrCu, the free-base TFcCorrH_3 was not isolated and copper insertion was performed immediately after the oxidative step in order to limit decomposition of the macrocycle. The UV−visible spectrum of DFcPhCorrCu (dotted line in Figure 3) is very similar to that of TFcCorrCu (solid line in Figure 3), both in the Soret and Q-band regions. On the other hand, the spectrum of FcDPhCorrCu (dashed line in Figure 3) is quite different, strongly resembling the published UV−visible spectrum of TPCorrCu,[38] although the Soret band of FcDPhCorrCu is slightly blue-shifted with respect to the bands of TFcCorrCu, while the Q band is significantly less intense in the triferrocenylcorrole and positioned around 650 nm. It is also interesting to note that, with an increase in the number of Fc substituents on the macrocycle, the intensity of the Soret band decreases while the Q band becomes more intense. This trend is seen in Figure 3 and also in Table 1, which summarizes data for the three Fc-functionalized copper corroles with those of the simple copper triphenylcorrole. The similarity in the spectroscopic data for TPCorrCu and FcDPhCorrCu compared to DFcPhCorrCu and TFcCorrCu confirms that substituents at the 5 and 15 positions of the macrocycle have a stronger effect on the UV−visible spectrum than does the substituent at the meso position 10.[40] This situation is quite different from what observed for similar porphyrins bearing a variable number of Fc and phenyl units. In this case, replacement of the phenyl rings with Fc moieties induces a red shift of the Soret band because of increased deviation from planarity of the porphyrin core.[41]

Table 1. Molar Absorption Coefficients (log ε) and Band Maxima (λ_{max}) of Copper Corrole Complexes in CH_2Cl_2

compound	Soret band (λ_{max})	Q band (λ_{max})
TPCorrCu	5.09 (410)	3.89 (538)
FcDPhCorrCu	5.01 (415)	3.90 (634)
DFcPhCorrCu	4.83 (420)	4.11 (667)
TFcCorrCu	4.75 (422)	4.14 (674)

The ^{1}H NMR spectra of FcDPhCorrCu and DFcPhCorrCu show four doublets (or sometimes a low resolved broad singlet) for the β-pyrrolic protons, which have resonance spread between 7.3 and 8.8 ppm; in all cases, they can be easily identified by the small coupling constant that is around 4 Hz, while the signal for the phenyl rings appears as a multiplet at around 7.5 ppm. There are three signals (1:1:2.5 ratio) for the α- and β-substituted and unsubstituted cyclopentadienyl ring in the 4−5 ppm region of the spectrum. The shape of the absorption for the hydrogen atoms of the Fc rings suggests that these substituents are free to rotate around, up and down with respect to the main plane of the corrole macrocycle, as was earlier reported for TFcCorrCu.[28]

To gain further insight into both the electronic structure and geometry of the complexes, density functional theory (DFT) analysis on TFcCorrCu was performed. The results of these calculations are described below.

Geometry optimizations and MO calculations were performed first on TFcCorrCu in order to elucidate the interactions, which occur between the *meso*-Fc groups and the corrole core. Copper corroles have been studied in detail from a theoretical point of view[39,42−44] because of their particular electronic configuration and geometric distortion of the core induced by the metal and in order to discuss the question of the noninnocence of the ligand. Different approaches have been used, including DFT calculations,[45−47] giving good results in terms of the geometric shape and extent of the electronic interaction that occurs between the macrocycle and coordinated central metal ion. The pure and hydrid GGA functionals give similar results to describe the geometry of copper corrole, but a different reason has been found as being responsible for saddling in the copper corrolates. In fact, using pure OLYP and BP86 functionals, a covalent Cu 3d−corrole π-type interaction was found, whereas using hybrid DFT functionals (B3LYP or PBE0), an antiferromagnetic coupling between an electron in the corrolate π and Cu^{II} 3d orbitals was found. This latter interaction seems to be more accurate in comparison with the ab initio calculations although with a larger contribution.[41] On the other hand, Fc-containing porphyrins have been studied using DFT calculations, and the best results, particularly those concerning the MO distributions, have been obtained using the pure GGA functional with Becke's exchange functional and the Perdew 86 or Perdew nonlocal correlation functional (BP86 or BPW91 GGA DFT functionals).[45−47]

For all of these reasons, to investigate the geometry and interaction between the Fc groups, the macrocycle core, and the copper ion of the currently investigated compounds, we decided to test first the different functionals on copper derivatives: pure, hybrid, and meta-pure GGA combinations, namely, BP86, OLYP, B3LYP, CAM-B3LYP, and TPSSTPSS. All of the tested functionals give comparable results in terms of the shape of the macrocycle, e.g., a saddled conformation as the most stable geometry (Figure 4), with a up−down−up arrangement of the *meso*-Fc substituents. Previous room temperature NMR experiments indicate, however, that in

DOI: 10.1021/acs.inorgchem.5b01575
Inorg. Chem. 2015, 54, 10256−10268

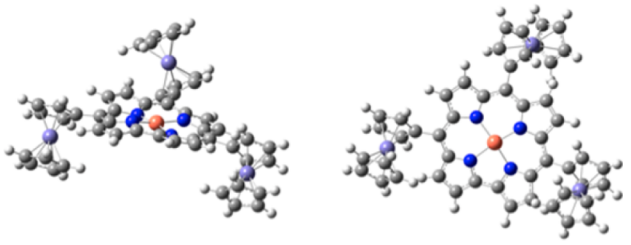

Figure 4. Front and top views of TFcCorrCu [geometry optimization at the BP86/6-31G(d,p) level of calculation].

solution the Fc units freely rotate around the *meso*-carbon atoms.[28]

The main difference between the various functionals concerns the contribution of different moieties to the orbital density. In fact, the results of OLYP, B3LYP, and CAM-B3LYP are inadequate to accurately describe the correct contribution to the overall MOs from the corrole core, the Fc groups, and the copper central metal. Using these functionals, the main contribution to the highest occupied molecular orbital (HOMO) is due to the Fc groups in positions 5 and 10, but this result is not corroborated by the absorption spectrum, where a strong contribution of the π-corrole core on the HOMO is clearly visible; this result is very different from what is seen for *meso*-ferrocenyl porphyrinoids, where the hybrid functional overestimates the π-macrocycle contributions to the HOMO and is quite unexpected for the OLYP approach.[40,42,45−47] The correct distribution of frontier orbitals is well described by the BP86 functional, as illustrated in Figure 5, while in Figure S6, the MO energy diagram is reported. Also,

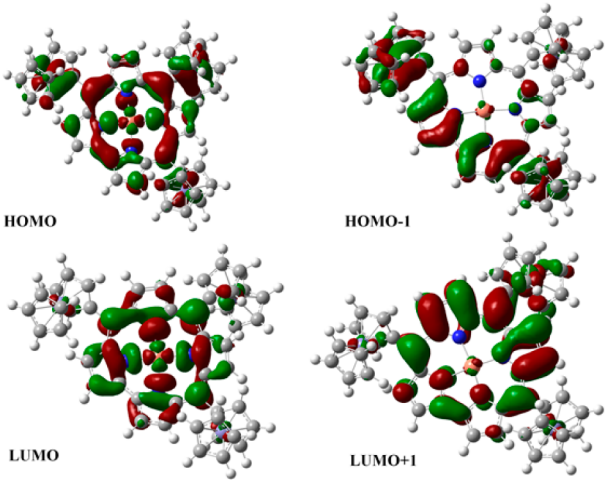

Figure 5. Frontier MO calculated for TFcCorrCu at the BP86/6-31G(d,p) level of calculation.

the meta GGA functional TPSSTPSS correctly allows for describing the orbital shapes in comparison with the experimental results. In fact, the HOMO is characterized by a strong interaction between the core, the Fc units, and the metal, as is seen from the experimentally measured absorption spectra. On the other hand, the unoccupied orbitals [lowest unoccupied molecular orbital (LUMO, LUMO+1, and LUMO+2)] are mainly centered on the macrocycle core.

In particular, the electronic properties are strongly influenced by substituents at the positions 5 and 15, and this can be clearly observed by analyzing the orbital contribution to the UV−visible spectra (Figure 5). In fact, the HOMO−1 contributes significantly to the Soret band absorption,[45,46] and a strong contribution from the Fc unit at the meso positions 5 and 15 is seen. This indicates that the Fc groups at these two positions mostly influence the electronic spectra compared to the Fc group at position 10, which has a smaller effect. This is in agreement with the similar absorption spectra of 5,15-DiFcPhCorrCu and TFcCorrCu, whereas the 10-position monosubstituted corrole FcDPhCorrCu has a UV−visible spectrum similar to that of other corrole derivatives with aromatic substituents. This behavior is in agreement with published results that underline the strong contribution of groups at the corrole meso positions 5 and 15 to the electronic spectrum compared to the smaller contribution from groups at the 10 position of the macrocycle.[40,48]

To further investigate the scope of the synthetic route for obtaining triferrocenylcorroles, we attempted to prepare the cobalt and nickel derivatives of $TFcCorrH_3$. In the case of $TFcCorrCo(PPh_3)$, the mixture containing $TFcCorrH_3$ was dissolved in $CHCl_3/CH_3OH$ along with an excess of $Co(AcO)_2$ and PPh_3 and stirred to reflux, while monitoring the course of the reaction by UV−visible spectroscopy and TLC analysis. After the desired complex was formed, chromatographic separation yielded a green fraction whose UV−visible spectrum is shown in Figure 6. This spectrum is very similar to that of

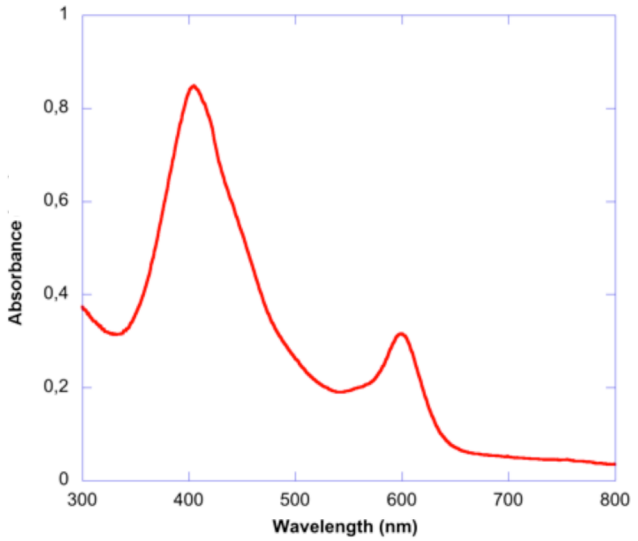

Figure 6. UV−visible spectrum of $TFcCorrCo(PPh_3)$ in CH_2Cl_2.

related cobalt triarylcorrolates,[49,50] and the formation of $TFcCorrCo(PPh_3)$ was confirmed by the mass spectrum, which exhibited a molecular peak at m/z 905, corresponding to the target triferrocenylcorrole after loss of the axial PPh_3 ligand.

The ^1H NMR spectrum of $TFcCorrCoPPh_3$ is shown in Figure 7, while Table S1 contains the observed chemical shifts and coupling constants. The assignments were obtained by a combination of $^1H-^1H$ COSY, $^1H-^1H$ ROESY, $^1H-^{13}C$ HSQC, and $^1H-^{13}C$ HMBC. An interesting feature in the spectra is the fact that two distinct signals are observed for the hydrogen and carbon atoms in position 2 of the 5/15-position Fc groups. The nonequivalence between these two positions is likely due to a restricted rotation of the Fc substituents in combination with a differentiation between the two faces of the corrole ring caused by the PPh_3 substituent. As a consequence, the two H-2 protons couple with each other, which is readily

DOI: 10.1021/acs.inorgchem.5b01575
Inorg. Chem. 2015, 54, 10256−10268

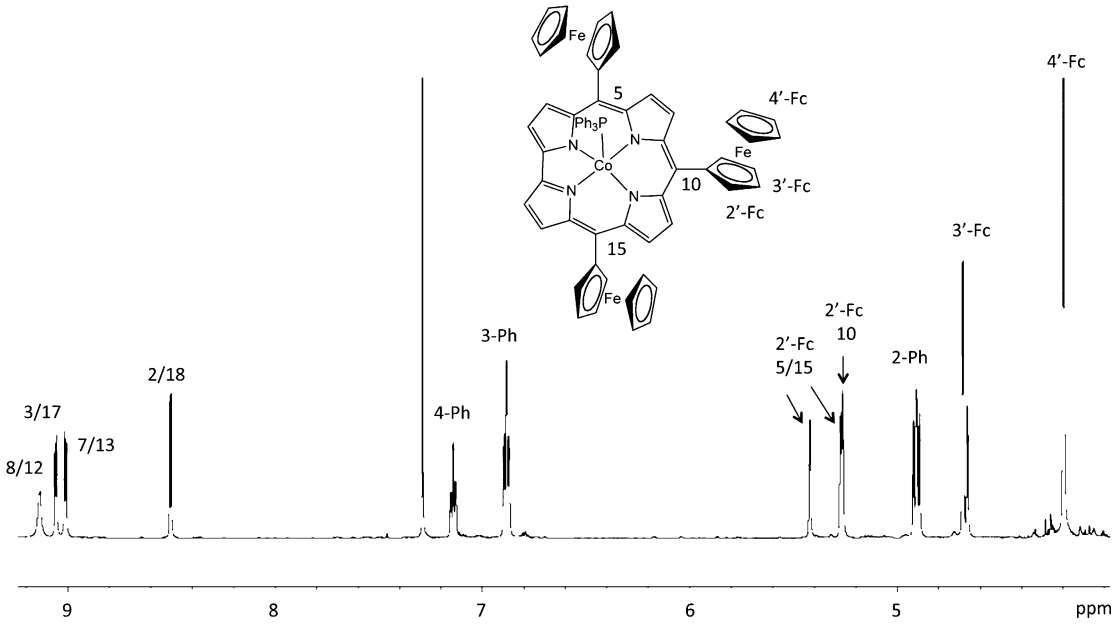

Figure 7. ^{1}H NMR spectrum of TFcCorrCo(PPh_3) in $CDCl_3$.

observed in the COSY spectrum (Figure S7) and yields two quartets, instead of the expected triplets that are normally observed for Fc protons of the substituted ring. On the other hand, only one signal is observed for protons of the 10-Fc group, for which a fast rotation is hypothesized. This suggests a particular conformation of the PPh_3 axial substituent that causes a larger steric hindrance for rotation of the Fc groups in positions 5 and 15 than in position 10. In fact, we observe in the ROESY spectrum a very short distance between the *o*-PPh_3 and *β*-pyrrolic protons in position 2/18. In this particular conformation, with one of the three Fc rings pointing toward the position 2/18, the 10-Fc is located in a relatively free region and rotates faster than the other two *meso*-Fc groups.

These results led us to investigate the geometry optimizations and MO calculations on TFcCorrCo(PPh_3), using the functional that gave a correct description of the copper complex, e.g., pure BP86. Quite surprisingly, the most stable atropoisomer has all three Fc groups on the same side of the molecule as the phosphine axial ligand, despite the steric hindrance potentially connected to this geometrical shape (see Figures 8, 9, and S6). This feature suggests some interaction

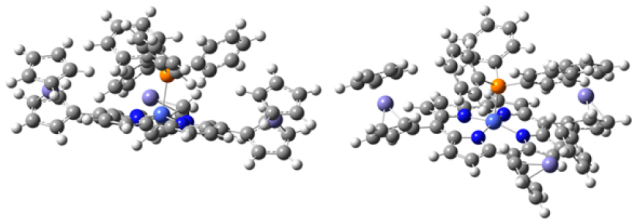

Figure 8. Molecular geometry calculated for TFcCorrCo(PPh_3) at the BP86/6-31G(d,p) level of calculation.

among the axial ligand and Fc groups, but future studies are needed to elucidate the nature of the interaction. A strong interaction between the *meso*-Fc groups, the central cobalt ion, and the corrole macrocycle can, however, be observed, and also in this case, the MOs are well described with the BP86 functional. Like in the case of TFcCorrCu, theoretical

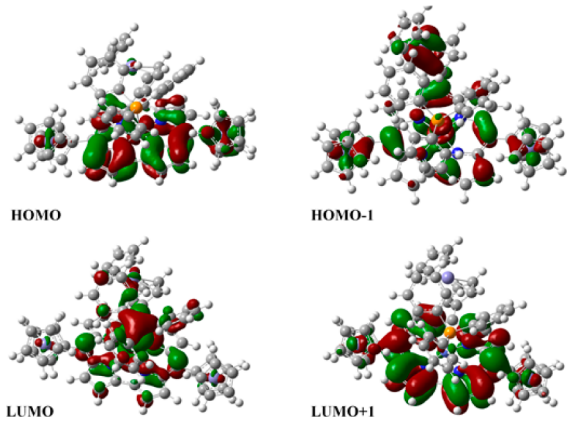

Figure 9. Frontier orbitals calculated for TFcCorrCo(PPh_3) at the BP86/6-31G(d,p) level of calculation.

calculations of the orbital distribution for TFcCorrCo(PPh_3) fit well the experimental results, and an interaction between the different Fc groups and the macrocycle is clearly visible.

The reaction of $TFcCorrH_3$ with nickel ions gave different and quite unexpected results. In an initial synthetic attempt to obtain the target molecule, the reaction mixture containing the free-base corrole and excess $Ni(AcO)_2$ was reacted at 80 °C in DMF because Fc derivatives are not stable at temperature higher than 90−100 °C. This procedure yielded mainly a green fraction, whose UV−visible spectrum was not characteristic of metalloporphyrin or metallocorrole (Figure S9). Formation of the desired TFcCorrNi was definitely ruled out by the ^{1}H NMR spectrum, which revealed the presence of a diamagnetic nickel(II) species, instead of a paramagnetic species, expected for TFcCorrNi. An initially intriguing result was the presence of only two Fc rings in the compound, as determined by signals in the 4−5 ppm region of the ^{1}H NMR spectrum. The presence of 10 signals (1 H each) between 5.9 and 8.2 ppm revealed the low symmetry of the molecule. The presence of high-field resonances of the *β*-pyrrolic protons indicated the absence of an aromatic macrocyclic system, which could be either due to

DOI: 10.1021/acs.inorgchem.5b01575
Inorg. Chem. 2015, 54, 10256−10268

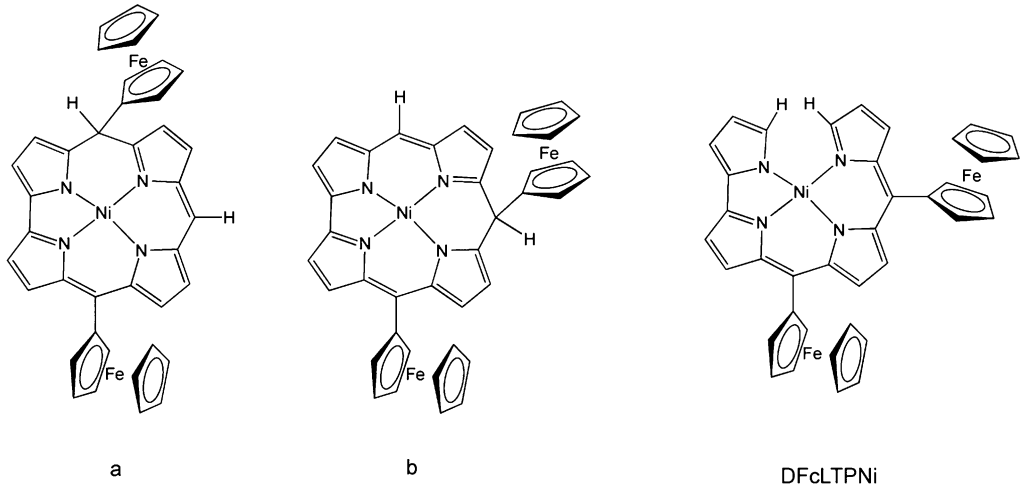

Figure 10. Structures of possible nickel isocorrole derivatives (a and b) and DFcLTPNi.

the formation of an isocorrole species,[51,52] as shown by the structures in Figure 10a,b, or due to a linear tetrapyrrolic complex.[53] The mass spectrum showed a molecular peak at m/z^+ 711, a value that did not match an isocorrole structure.

A definitive structure of the nickel derivative was then confirmed by NMR analysis as the open-chain complex DFcLTPNi illustrated in Figure 2 (NMR data are reported in Table S2). The ^{1}H NMR spectrum of DFcLTPNi (Figure S10) shows the presence of only two Fc substituents. The COSY spectrum of DFcLTPNi in the region of 5.9−8.2 ppm shows the presence of four spin systems, two comprising two hydrogen atoms, and two others with three hydrogen atoms (Figure S11). This indicates that two of pyrrolic rings on the compound bear three hydrogen atoms. Analysis of the ^{1}H−^{1}H ROESY spectrum allowed for the assignment of all β-pyrrolic signals and corroborated the proposed structure shown in Figure 10. In this experiment, a very intense cross-peak was observed between the hydrogen atoms in positions 14 and 15, in line with their short distance in the proposed structure.

The measured coupling constants are shown in Table S3 and, in the case of the two rings with three hydrogen atoms, follow the expected trend for the J values observed for pyrrole ($^3J_{3,4} > {}^3J_{2,3} > {}^4J_{2,4}$).[54] Chemical shifts for the ^{1}H and ^{13}C nuclei, based on COSY, ROESY, ^{1}H−^{13}C HSQC, and ^{1}H−^{13}C HMBC experiments, are shown in Table S2.

The formation of such a product is quite unexpected because the opening of the corrole macrocycle is usually accompanied by oxidation to an open-chain derivative, leading to the formation of a biliverdine-like compound[55,56] when it occurs at the pyrrole−pyrrole direct link. When the ring opening has been observed at the 5 position, a benzoyl group was the substituent observed at the terminal α-pyrrolic position.[57] In our case, the ring opening is not oxidative and no oxygen insertion has been observed at the peripheral position of the linear tetrapyrrole. Attempts were made to coordinate nickel ion by using mild reaction conditions and Ni(AcO)$_2$ in refluxing CH_2Cl_2/CH_3OH, but the only isolable reaction product was again DFcLTPNi and the expected triferrocenylcorrole complex was not isolated.

Electrochemistry of Copper Complexes. The electrochemistry of each copper ferrocenylcorrole was examined in PhCN containing 0.1 M tetrabutylammonium perchlorate (TBAP) as the supporting electrolyte. Examples of cyclic voltammograms in this solvent are illustrated in Figure 11, and a summary of the $E_{1/2}$ values for each redox reaction under

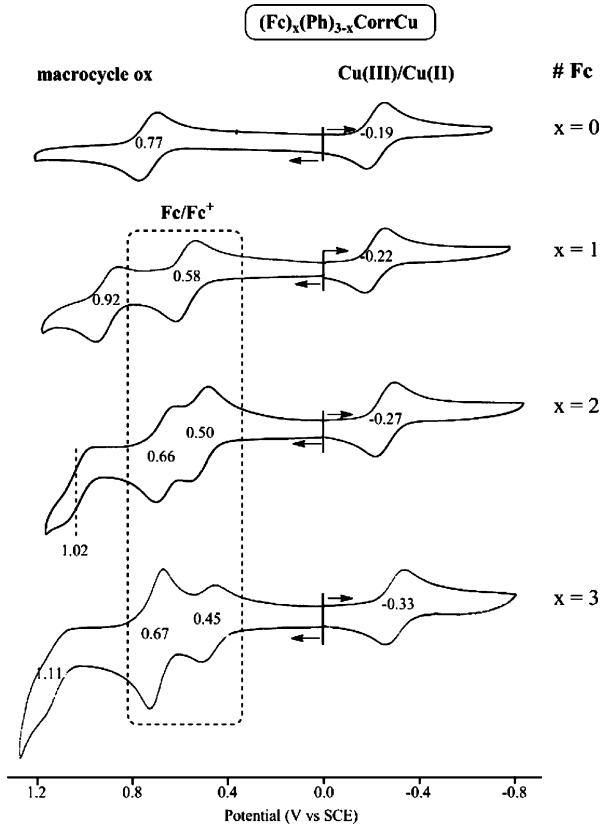

Figure 11. Cyclic voltammograms of (Fc)$_x$(Ph)$_{3-x}$CorrCu, where x = 0−3 in PhCN, containing 0.1 M TBAP at a scan rate of 0.1 V/s.

these solution conditions is given in Table 2. For comparison purposes, potentials for oxidation and reduction of the related non-Fc derivative, 5,10,15-triphenylcorrole (TPCorr), are also given in the figure and table.

The reversible redox reactions in Figure 11 can be assigned to three sites of electron addition or electron abstraction, as indicated in the figure. One site of electron transfer involves the macrocycle, which is reversibly oxidized at $E_{1/2}$ values between 0.77 and 1.11 V. The second is oxidation of the Fc groups,

DOI: 10.1021/acs.inorgchem.5b01575
Inorg. Chem. 2015, 54, 10256−10268

Table 2. Half-Wave Potentials (V vs SCE) for Copper Ferrocenylcorroles in PhCN, Containing 0.1 M TBAP

		ox (macrocycle)	ox (Fc)			red (Cu^{III}/Cu^{II})
compound	#Fc[a]	first	third	second	first	first
TPCorrCu	0	0.77				−0.19
FcDPhCorrCu	1	0.92			0.58	−0.22
DFcPhCorrCu	2	1.02		0.66	0.50	−0.27
TFcCorrCu	3	1.11	0.67	0.67	0.45	−0.33

[a]Number of Fc groups on the macrocycle.

which occurs at $E_{1/2}$ values between 0.45 and 0.67 V, and the third site of electron transfer involves reduction of the copper(III) central metal ion to its copper(II) form at $E_{1/2}$ = −0.19 to −0.33 V.

The neutral corrole formally contains copper(III), and the first reduction process can then be described as electron addition to the central metal ion, forming $TFcCorrCu^{II}$ as a final reduction product. The alternate assignment of the neutral compound as a copper(II) corrole π-cation radical[39,40,42−44] cannot be ruled out, although the exact nature of the assignment has no bearing on the product of the one-electron reduction, which unambiguously contains copper(II) in each compound.

A second reduction of TFcCorrCu is also observed at $E_{1/2}$ = −2.03 V in PhCN and −1.97 V in DMF (see Figure S12). This process involves electron addition to the conjugated macrocycle, forming a copper(II) corrole π-anion radical. This reduction behavior is similar to that of other previously investigated copper corrole derivatives.[35,58−60] Fc is a strong electron-donating group, and thus the stepwise replacement of each *meso*-phenyl group in TPCorrCu by a Fc substituent results in a systematic negative shift in the potential for the first reduction, whose $E_{1/2}$ value is directly proportional to the number of Fc groups on the compound. This is graphically shown in Figure 12, where the reversible first reduction potential shifts from −0.19 V for the copper(III)/copper(II) reaction of TPCorrCu to −0.33 V for the same electrode reaction of TFcCorrCu.

A systematic negative shift in $E_{1/2}$ is also seen for the first one-electron oxidation of each ferrocenylcorrole as the number of Fc groups on the macrocycle is increased, from one in the case of FcDPhCorrCu to three in the case of TFcCorrCu. The potential of 0.58 V for the reversible conversion of Fc to Fc^+ on

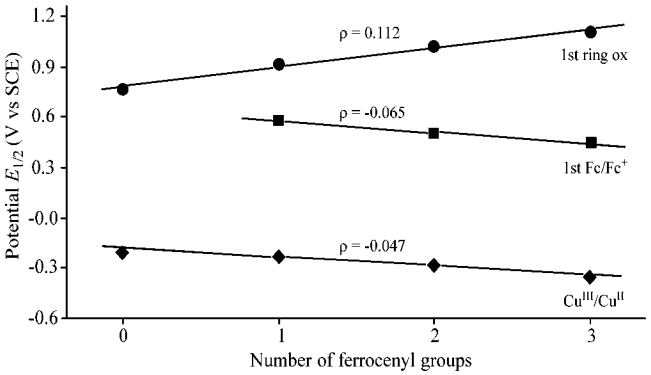

Figure 12. Relationship between the measured redox potentials of copper corroles and the number of Fc groups on the molecule.

FcDPhCorrCu (x = 1) is more difficult by 100 mV than the measured $E_{1/2}$ value for the oxidation of free Fc under the same solution conditions ($E_{1/2}$ = 0.48 V). The reversible oxidation of one Fc group on DFcPhCorrCu (x = 2) is located at $E_{1/2}$ = 0.50 V, and this potential is also more positive than the $E_{1/2}$ value of unlinked Fc in this solvent. Only in the case of TFcCorrCu is the Fc/Fc^+ process easier than that of the free Fc. This first oxidation of TFcCorrCu occurs at $E_{1/2}$ = 0.45 V in PhCN, and a plot of the half-wave potential for the first Fc-centered oxidation versus the number of Fc groups on the compound is again linear, as shown in Figure 12.

DFcPhCorrCu (x = 2) undergoes three one-electron oxidations, the first two of which are ascribed to the oxidation of Fc substituents at the 5 and 15 positions of the macrocycles. The second Fc group oxidation on DFcPhCorrCu (x = 2) is harder (occurs at a more positive potential) than the first by 160 mV, and the separation in potential between the two Fc/Fc^+ processes is consistent with an interaction between the two equivalent redox-active groups of the complex.[61−63]

Three reversible oxidations of $TFcCorrCu^{III}$ can be observed within the positive potential window of PhCN. These occur at $E_{1/2}$ = 0.45, 0.67, and 1.11 V, respectively. The current height for the second oxidation of TFcCorrCu at $E_{1/2}$ = 0.67 V is twice that of the other processes (see Figure 11), indicating two overlapping one-electron oxidations at the same potential. As indicated above, the unlinked Fc molecule exhibits a reversible one-electron oxidation at $E_{1/2}$ = 0.48 V in PhCN, and this potential can be compared to the $E_{1/2}$ = 0.45 V for the first one-electron oxidation of TFcCorrCu, where the process is proposed to involve electron abstraction from the Fc group located at the meso position 10 of the macrocycle.

The process at $E_{1/2}$ = 0.67 for TFcCorrCu (x = 3) involves two overlapping one-electron oxidations and is assigned to the abstraction of one electron from the equivalent Fc groups at the meso positions 5 and 15 of the macrocycle. The fact that the half-wave potential for the first oxidation of $TFcCorrCu^{III}$ (0.45 V) is very close to the $E_{1/2}$ value of Fc itself in PhCN (0.48 V) is consistent with the spectroscopic and theoretical data that indicate little communication between this Fc group at the meso position 10 of the macrocycle and the conjugated π-ring system of the corrole. On the other hand, the potentials for oxidation of the other two Fc groups at the meso positions 5 and 15 are positively shifted by 190 mV from the $E_{1/2}$ value for the oxidation of free Fc, and this is consistent with a strong interaction occurring between the two unoxidized *meso*-Fc substituents and the positively charged Fc^+ group, generated in the redox process at 0.45 V. From this point of view, Fc-based copper and cobalt corroles (see the later section of the text) behave similarly to the corresponding copper (and cobalt) complex of TFcPorph, where a certain degree of electronic communication has been observed by electrochemical measures.[64] Anyway it should be noted that, in the case of porphyrin derivatives, the potentials recorded for each Fc oxidation have been obtained using a different solvent/supporting electrolyte system.

The first macrocycle-centered oxidation of the triphenylcorrole TPCorrCu is observed at $E_{1/2}$ = 0.77 V in PhCN, and this potential can be compared to a similar macrocycle-centered oxidation of the triferrocenylcorrole complex, TFcCorrCu, at $E_{1/2}$ = 1.11 V. The presence of the three electron donating *meso*-Fc groups might be expected to lead to easier oxidations of TFcCorrCu compared to those of TPCorrCu, but the effect of the electron-donating substituents is counterbalanced by the

DOI: 10.1021/acs.inorgchem.5b01575
Inorg. Chem. 2015, 54, 10256−10268

positive charges on the ferrocenium groups of the singly, doubly, and triply oxidized complexes, thus resulting in much harder ring-centered oxidations of the three ferrocenylcorrole derivatives compared to the same electrode reaction of TPCorrCu, which is uncharged when converted to a corrole π-radical cation at 0.77 V. Each added positive charge shifts $E_{1/2}$ for oxidation of the macrocycle toward a more positive potential, and a plot of $E_{1/2}$ for this process versus the number of Fc groups is linear, as shown in Figure 12. The difference in the potential between the macrocycle-centered oxidation of TPCorrCu and the same redox reaction of TFcCorrCu amounts to 340 mV, and as described later in the manuscript, the same positive shift of the potential is observed for the two structurally related cobalt complexes.

Spectra of Electroreduced and Electrooxidized Copper Corroles. UV−visible spectra were monitored during the first reduction and first oxidation of each copper corrole, in order to further elucidate the site of electron transfer and also evaluate the effect of the *meso*-Fc substituents on the UV−visible spectra of the compounds in their neutral, singly reduced and singly oxidized forms. Examples of the relevant cyclic voltammograms for the four copper complexes are given in Figure 11, and the relevant spectral changes, obtained in the thin-layer cell during the first one-electron addition and first one-electron abstraction, are shown in Figures 13 and 14, respectively.

The spectral changes in Figure 13 are in each case consistent with a copper(III)/copper(II) process. The formal conversion of copper(III) corrole to its copper(II) form is accompanied by a 22 nm red shift in the Soret band position for TPCorrCu (Figure 13a), and a 18−23 nm red shift is also seen for the three Fc derivatives (Figure 13b−d), with the main difference between the four sets of spectral changes being the generation of copper(II) corrole characterized by a decreasing intensity and broadened Soret band with increase in the number of Fc groups on the compound. All four electrogenerated copper(II) corroles possess two moderately intense Q bands, as seen in the figure, with the most intense band shifting more and more toward the red with each added Fc group. The exact wavelengths of the Soret and Q bands for the neutral and electroreduced copper corroles are summarized in Table 3.

Of most significance are the spectral changes seen upon the first one-electron oxidation of the same series of corroles in PhCN. The first oxidation of each compound involves a reversible one-electron abstraction (as seen by cyclic voltammograms in Figure 11), but the site of electron transfer is different in the two series of compounds, being ring-centered in the case of TPCorrCu and Fc-centered in the case of FcDPhCorrCu, DFcPhCorrCu, and TFcCorrCu. As such, one might anticipate a radical-type UV−visible spectrum in the case of singly oxidized TPCorrCu and very few spectral changes to occur for the other singly oxidized compounds, where the reaction involves a *meso*-Fc substituent on the molecule. However, this is not what was experimentally observed, as seen in Figure 14, where a significant loss of the Soret band intensity is observed upon each one-electron oxidation, along with a loss of the Q band in the case of DFcPhCorrCu and TFcCorrCu (Figure 14c,d). The large decrease of the Soret band intensity after oxidation of a single Fc substituent indicates a significant transfer of positive charge from the singly oxidized ferrocenium group to the π-ring system of the corrole. The spectral changes accompanying the oxidation of unlinked Fc are given in Figure S13 and are characterized by the presence of a new absorption

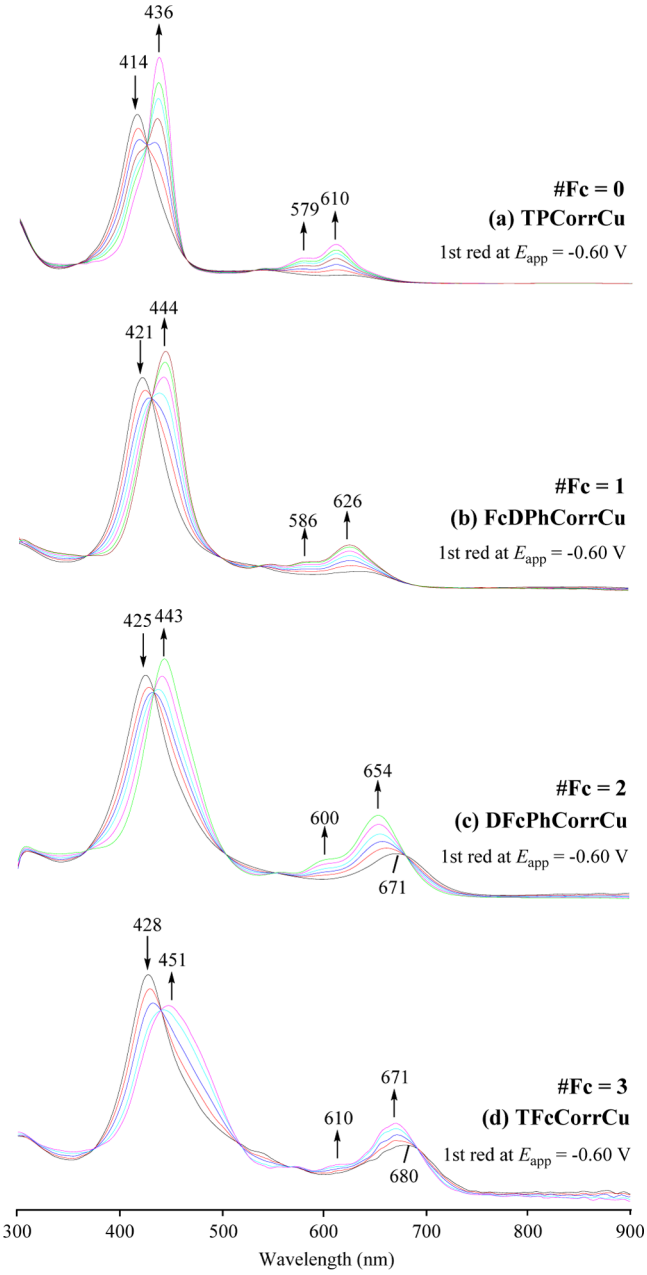

Figure 13. UV−visible spectral changes during controlled potential reduction of (a) TPCorrCu, (b) FcDPhCorrCu, (c) DFcPhCorrCu, and (d) TFcCorrCu to their singly reduced forms in PhCN containing 0.1 M TBAP. The applied reducing potential was −0.60 V in each case.

at about 600 nm. This band is not observed in the spectrum of singly oxidized FcDPhCorrCu, DFcPhCorrCu, or TFcCorrCu, again indicating a significant coupling between the positive charge on Fc^+ and the π-ring system of the macrocycle.

Electrochemistry of Cobalt Complexes. The mechanism for reduction of TFcCorrCo(PPh_3) is similar to that of previously investigated cobalt corroles containing a bound PPh_3 axial ligand.[60−64] The first reduction is quasi-reversible and involves the conversion of TFcCorrCo^{III}(PPh_3) to [TFcCorrCo^{II}(PPh_3)]$^-$, followed by rapid dissociation of the axially bound PPh_3 ligand to generate the anionic four-coordinate cobalt(II) corrole, [TFcCorrCo^{II}]$^-$ (an electrochemical EC mechanism). The four-coordinate cobalt(II) corrole can be further reduced to its cobalt(I) form at −1.71 V, as shown by

DOI: 10.1021/acs.inorgchem.5b01575
Inorg. Chem. 2015, 54, 10256−10268

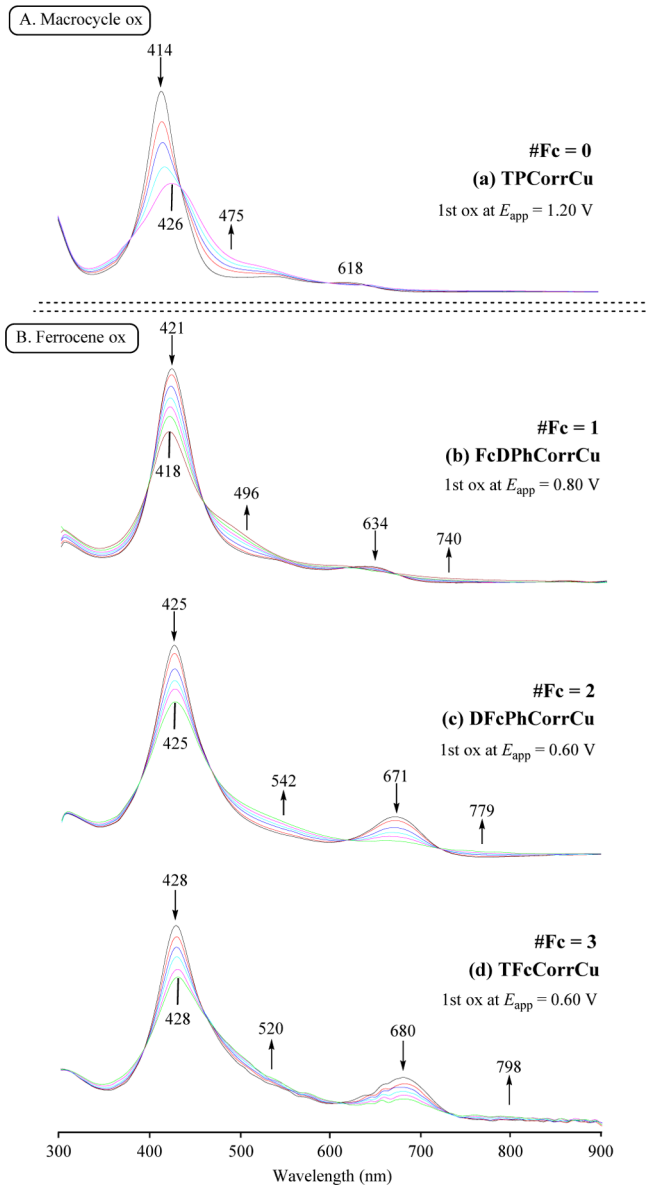

Figure 14. UV−visible spectral changes during the first one-electron-controlled potential oxidation of (a) TPCorrCu, (b) FcDPhCorrCu, (c) DFcPhCorrCu, and (d) TFcCorrCu in PhCN containing 0.1 M TBAP. The site of electron transfer is the macrocycle for TPCorrCu (#Fc = 0) and a *meso*-Fc substituent for the other compounds.

the cyclic voltammogram in Figure 15. The unligated cobalt(II) corrole can also be irreversibly reoxidized via an electrochemical EC mechanism to give first a transient four-coordinate $TFcCorrCo^{III}$ species, followed by re-formation of the neutral five-coordinate cobalt(III) corrole with a coordinated triphenylphosphine axial ligand, as shown in Scheme 1.

Although the mechanism shown in Scheme 1 for $TFcCorrCo^{III}(PPh_3)$ is the same as that previously reported for $TPCorrCo^{III}(PPh_3)$,[15,40,65−67] there is not a large effect of the three Fc groups on the peak potential for conversion of cobalt(III) to cobalt(II). As seen in Figure 16, the first reduction peak potential has been shifted from E_p = −0.75 V for the TPCorr complex in PhCN to −0.78 V for the TFcCorr derivative in the same solvent. The second metal-centered reduction of cobalt corrole is also insensitive to the electron-donating Fc substituents, as indicated by the fact that $TFcCorrCo^{II}$ and $TPCorrCo^{II}$ are both reversibly reduced to their Co^{I} form at an identical potential of $E_{1/2}$ = −1.71 V. In contrast, the expected substituent effect is seen in the peak potential for reoxidation of the singly reduced corrole. This potential shifts from E_{pc} = −0.10 V for TPCorr to −0.26 V for TFcCorr.

It is important to note that potentials for the three Fc-centered oxidations of $TFcCorrCo(PPh_3)$ are almost identical with the $E_{1/2}$ values for the three Fc oxidations of TFcCorrCu. The first electron abstraction from $TFcCorrCo(PPh_3)$ is proposed to involve the Fc group at position 10 and occurs at $E_{1/2}$ = 0.42 V; the following two-electron abstractions are then proposed to occur at the Fc groups located at positions 5 and 15, and this redox process occurs at $E_{1/2}$ = 0.62 V. The separation between the $E_{1/2}$ values for the two sets of Fc-centered oxidations is 200 mV, which is very similar to $\Delta E_{1/2}$ = 220 mV for the same two Fc-centered redox processes of TFcCorrCu. However, as seen in Figure 15, the first and second oxidations of $TFcCorrCo(PPh_3)$ have similar current heights, thus suggesting that the first oxidation process actually involves two overlapping one-electron transfers. We propose that one electron in the first step is abstracted from the Fc group (at the 10 position) and the other from the metal center of the cobalt corrole [a cobalt(III)/cobalt(IV) process] at the same potential of 0.42 V. Two additional overlapping one-electron transfers, both involving the unoxidized Fc groups, are then observed at $E_{1/2}$ = 0.62 V, and this is followed by the stepwise one-electron transfers of the conjugated macrocycle at 0.92 and 1.28 V, respectively. It should be noted that the 330−360 mV shift in $E_{1/2}$ between the two macrocycle-centered oxidations of $TPCorrCo(PPh_3)$ and $TFcCorrCo(PPh_3)$ is similar to the earlier described 340 mV separation between the related redox reactions of TPCorrCu and TFcCorrCu.

Spectra of Electroreduced and Electrooxidized Cobalt Corroles. A comparison of the spectral changes that occur

Table 3. UV−Visible Spectral Data (λ_{max} and log ε) of Neutral, Singly Oxidized and Singly Reduced $CorrCu^{III}$ in PhCN Containing 0.1 M TBAP

		λ_{max}, nm (log ε, M^{-1} cm^{-1})					
		$[CorrCu^{III}]^{+}$ [a]	$CorrCu^{III}$		$[CorrCu^{II}]^{-}$		
compound	#Fc	Soret band	Soret band	Q band	Soret band	Q band	
TPCorrCu	0	426 (4.89)	414 (5.15)	624 (3.86)	436 (5.23)	579 (4.29)	610 (4.47)
FcDPhCorrCu	1	418 (4.51)	421 (4.91)	634 (4.05)	444 (4.98)	586 (4.00)	626 (4.22)
DFcPhCorrCu	2	425 (4.59)	425 (4.87)	671 (4.09)	443 (4.80)	600 (4.02)	654 (4.35)
TFcCorrCu	3	428 (4.67)	428 (4.80)	680 (4.19)	451 (4.73)	610 (3.97)	671 (4.32)

[a]In the absence of Fc substituents (#Fc = 0), the first oxidation occurs on the macrocycle, while in all other cases (#Fc = 1, 2, or 3), a Fc substituent is the site of electron abstraction.

DOI: 10.1021/acs.inorgchem.5b01575
Inorg. Chem. 2015, 54, 10256−10268

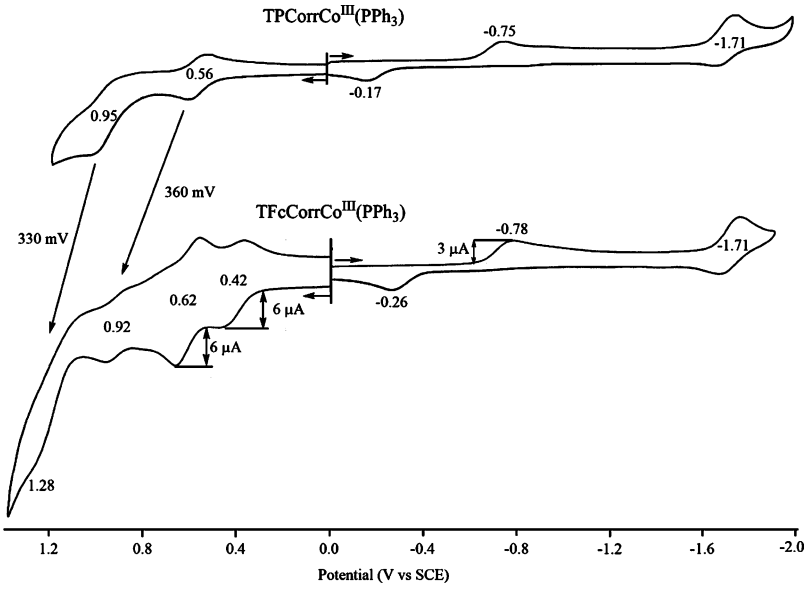

Figure 15. Cyclic voltammograms of $TPCorrCo^{III}(PPh_3)$ and $TFcCorrCo^{III}(PPh_3)$ in PhCN containing 0.1 M TBAP at a scan rate of 0.1 V/s.

Scheme 1. Proposed Mechanisms for Reduction of $TFcCorrCo^{III}(PPh_3)$ in PhCN Containing 0.1 M TBAP

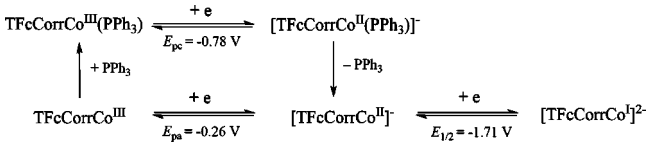

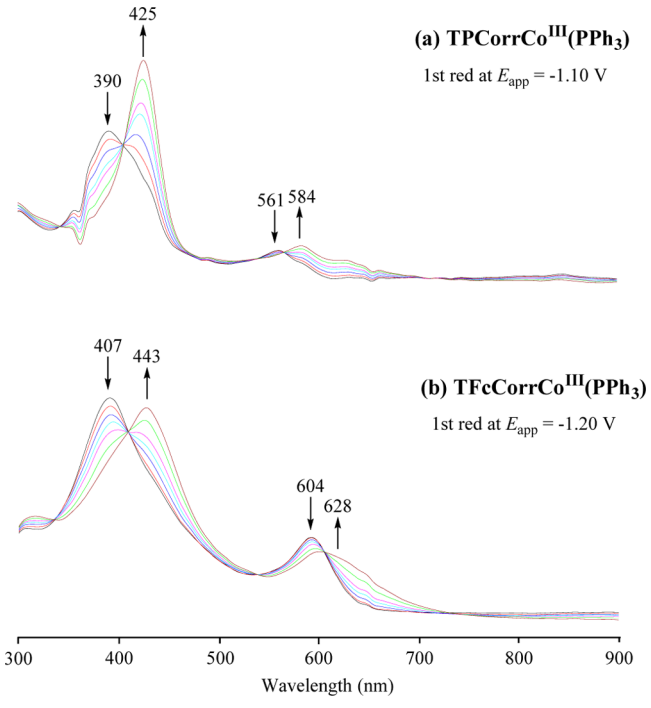

Figure 16. UV−visible spectral changes during the controlled potential reduction of (a) $TPCorrCo^{III}(PPh_3)$ and (b) $TFcCorrCo^{III}(PPh_3)$ in PhCN containing 0.1 M TBAP.

upon conversion of cobalt(III) to cobalt(II) in the triferrocenyl- and triphenylcorrole derivatives is shown in Figure 16. The Soret band shifts to the red by 35−36 nm for both compounds upon reduction, and both cobalt(II) corrole products possess a Q band that is also red-shifted by 23−24 nm compared to the initial compounds in their cobalt(III) form. These spectral changes are as expected for a metal-centered electron transfer, in this case cobalt(III) to cobalt(II).

Similar types of spectral changes are seen during the global two-electron oxidation of $TFcCorrCo(PPh_3)$ at $E_{1/2}$ = 0.42 V and the one-electron oxidation of $TPCorrCo(Ph_3)$ at 0.56 V. A metal-centered Co^{III}/Co^{IV} process has been suggested in the case of the triphenylcorrole,[49] and the spectral changes shown in Figure 17 are consistent with this assignment. The fact that similar spectral changes are observed upon the two-electron

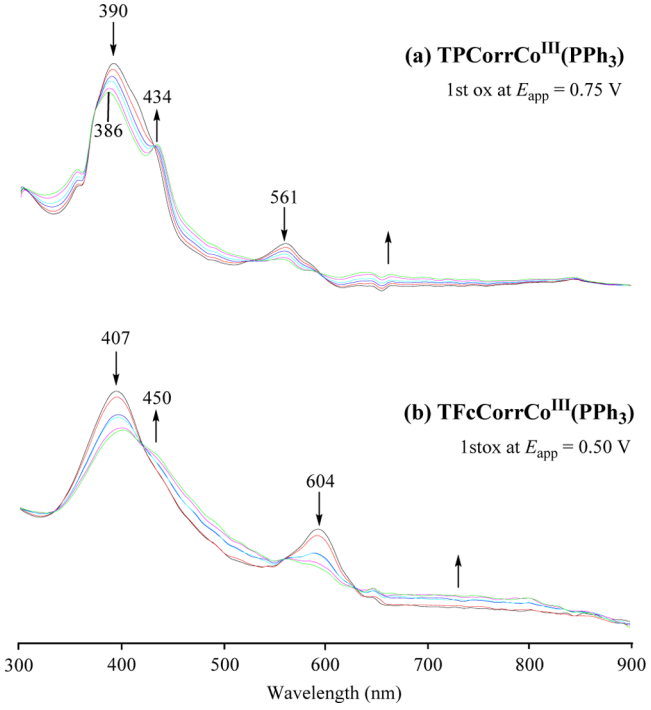

Figure 17. UV−visible spectral changes during the controlled potential oxidation of (a) $TPCorrCo^{III}(PPh_3)$ and (b) $TFcCorrCo^{III}(PPh_3)$ in PhCN containing 0.1 M TBAP.

DOI: 10.1021/acs.inorgchem.5b01575
Inorg. Chem. 2015, 54, 10256−10268

Scheme 2. Proposed Mechanism for the oxidation of TFcCorrCu and TFcCorrCo(PPh_3) in PhCN Containing 0.1 M TBAP

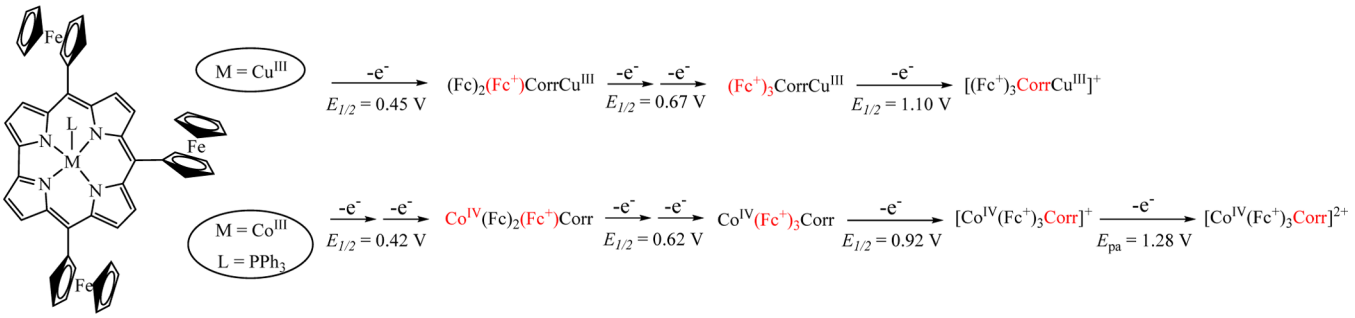

oxidation of TFcCorrCo(PPh_3) and the one-electron oxidation of TPCorrCo(PPh_3) can be interpreted in terms of one electron being abstracted from the central cobalt ion and the other from one of the three Fc groups on the triferrocenyl compound. A band close to 600 nm, which can be assigned to Fc^+, is not detected in the spectrum of the electrooxidized cobalt corrole, but the loss of the intense Q band in the electrooxidized product provides further evidence for conversion of one Fc group to its Fc^+ form.

In summary, the proposed overall mechanism for the oxidation of TFcCorrCo(PPh_3) and TFcCorrCu is given in Scheme 2.

CONCLUSIONS

We report herein a synthetic pathway that allows the preparation of metal derivatives of TFcCorr, together with a detailed study of the corresponding electrochemical and spectral properties of the compound in their neutral, singly oxidized and singly reduced forms. Theoretical, spectroscopic, and electrochemical characterization of the copper and cobalt ferrocenyl derivatives demonstrates that Fc groups at the 5 and 15 positions of the macrocycle interact more strongly with the corrole π-ring system than does the Fc substituent at the 10 position. DFT calculations indicated the up−down−up conformer as the most stable atropoisomer of TFcCorrCu, although free rotation of the Fc groups around the *meso*-carbon atoms is observed by NMR. On the other hand, DFT calculations of TFcCorrCo(PPh_3) indicate that the most stable conformer has all three Fc groups on the same side of the macrocyclic plane as the PPh_3 ligand, while NMR characterization of the compound in solution shows that steric hindrance due to the PPh_3 group hampers rotation of the Fc units at the 5 and 15 positions of the macrocycle. Attempts to prepare the nickel complex of TFcCorr following the same synthetic pathway as that for the copper or cobalt derivatives gave a different result, showing an opening of the corrole ring, with a loss of a methine bridge to give a diferrocenyl-substituted linear nickel tetrapyrrole complex.

ASSOCIATED CONTENT

Supporting Information

The Supporting Information is available free of charge on the ACS Publications website at DOI: 10.1021/acs.inorgchem.5b01575.

Electrochemistry of DFcLTPNi, ^1H NMR, FAB MS data, 2D ^1H−^1H COSY and UV−visible spectra, and cyclic voltammograms of compounds (PDF)

AUTHOR INFORMATION

Corresponding Authors

*Tel: +1 (713) 743-2740. Fax: +1 (713) 743-2745. E-mail: kkadish@uh.edu (K.M.K.).

*Tel: +39 (06) 72594752. Fax: +39 (06) 72594328. E-mail: roberto.paolesse@uniroma2.it (R.P.).

Notes

The authors declare no competing financial interest.

ACKNOWLEDGMENTS

This work is dedicated to Professor Barbara Floris on the occasion of her retirement. Thanks are given to PRIN 2010−2011 (to P.G.) and to the Robert A. Welch Foundation (Grant E-680 to K.M.K.).

REFERENCES

(1) Battersby, A. R.; McDonald, E. In *Porphyrins and Metalloporphyrins*; Smith, K. M., Ed.; Elsevier: Amsterdam, The Netherlands, 1975; pp 61−122.

(2) Che, C. M.; Lo, V. K.-Y.; Zhou, C.-Y.; Huang, J.-S. *Chem. Soc. Rev.* **2011**, *40*, 1950−1975.

(3) Paolesse, R.; Monti, D.; Nardis, S.; Di Natale, C. In *The Handbook of Porphyrin Sciences*; Kadish, K. M., Smith, K. M., Guilard, R., Eds.; World Scientific Publishing Co.: Singapore, 2011; Vol *12*, pp 121−225.

(4) Guldi, D. M. *Chem. Soc. Rev.* **2002**, *31*, 22−36.

(5) Lang, K.; Mosinger, J.; Wagnerová, D. M. *Coord. Chem. Rev.* **2004**, *248*, 321−350.

(6) Ormond, A. B.; Freeman, H. S. *Materials* **2013**, *6*, 817−840.

(7) Walter, M. G.; Rudine, A. B.; Wamser, C. C. *J. Porphyrins Phthalocyanines* **2010**, *14*, 759−792.

(8) Vecchi, A.; Galloni, P.; Floris, B.; Nemykin, V. N. *J. Porphyrins Phthalocyanines* **2013**, *17*, 165−196.

(9) Vecchi, A.; Galloni, P.; Floris, B.; Dudkin, S.; Nemykin, V. N. *Coord. Chem. Rev.* **2015**, *291*, 95−171.

(10) Nardis, S.; Monti, D.; Paolesse, R. *Mini-Rev. Org. Chem.* **2005**, *2*, 355−374.

(11) Barata, J. F. B.; Santos, C. I. M.; Neves, M. G. P. M. S.; Amparo, M. A. F.; Cavaleiro, J. A. S. *Synthesis and Modification of Porphyrinoids—Topics in Heterocyclic Chemistry*; Paolesse, R., Ed.; Springer: New York, 2014; Vol. *33*, pp 79−114.

(12) Liu, H. Y.; Mahmood, M. H. R.; Qiu, S. X.; Chang, C. K. *Coord. Chem. Rev.* **2013**, *257*, 1306−1333.

(13) Lemon, C. M.; Dogutan, D. K.; Nocera, D. G. In *The Handbook of Porphyrin Sciences*; Kadish, K. M., Smith, K. M., Guilard, R., Eds.; World Scientific Publishing Co.: Singapore, 2011; Vol *21*, pp 1−144.

(14) Schechter, A.; Stanevsky, M.; Mahammed, A.; Gross, Z. *Inorg. Chem.* **2012**, *51*, 22−24.

(15) Ou, Z.; Lü, A.; Meng, D.; Huang, S.; Fang, Y.; Lu, G.; Kadish, K. M. *Inorg. Chem.* **2012**, *51*, 8890−8896.

(16) Lei, H.; Fang, H.; Han, Y.; Lai, W.; Fu, X.; Cao, R. *ACS Catal.* **2015**, *5*, 5145−5153.

DOI: 10.1021/acs.inorgchem.5b01575
Inorg. Chem. 2015, 54, 10256−10268

(17) Tortora, L.; Pomarico, G.; Nardis, S.; Martinelli, E.; Catini, A.; D'Amico, A.; Di Natale, C.; Paolesse, R. *Sens. Actuators, B* **2013**, *187*, 72−77.
(18) Walker, D.; Chappel, S.; Mahammed, A.; Brunschwig, B. S.; Winkler, J. R.; Gray, H. B.; Zaban, A.; Gross, Z. *J. Porphyrins Phthalocyanines* **2006**, *10*, 1259−1262.
(19) Flamigni, L.; Gryko, D. T. *Chem. Soc. Rev.* **2009**, *38*, 1635−1646.
(20) Salvatori, P.; Amat, A.; Pastore, M.; Vitillaro, G.; Sudhakar, K.; Giribabu, L.; Soujanya, Y.; De Angelis, F. *Comput. Theor. Chem.* **2014**, *1030*, 59−66.
(21) Barata, J. F. B.; Zamarrón, A.; Neves, M. G. P. M. S.; Faustino, M. A. F.; Tomé, A. C.; Cavaleiro, J. A. S.; Röder, B.; Juarranz, Á.; Sanz-Rodriguez, F. *Eur. J. Med. Chem.* **2015**, *92*, 135−144.
(22) Haber, A.; Gross, Z. *Chem. Commun.* **2015**, *51*, 5812−5827.
(23) Ghosh, A.; Wondimagegn, T.; Parusel, A. B. J. *J. Am. Chem. Soc.* **2000**, *122*, 5100−5104.
(24) Stefanelli, M.; Nardis, S.; Tortora, L.; Fronczek, F. R.; Smith, K. M.; Licoccia, S.; Paolesse, R. *Chem. Commun.* **2011**, *47*, 4255−4257.
(25) Palmer, J. H. *Struct. Bonding (Berlin, Ger.)* **2011**, *142*, 49−90.
(26) Day, P.; Hush, N. S.; Clark, R. J. H. *Philos. Trans. R. Soc., A* **2008**, *366*, 5−14.
(27) Hadt, R. G.; Nemykin, V. N. *Inorg. Chem.* **2009**, *48*, 3982−3992.
(28) Pomarico, G.; Vecchi, A.; Mandoj, F.; Bortolini, O.; Cicero, D. O.; Galloni, P.; Paolesse, R. *Chem. Commun.* **2014**, *50*, 4076−4078.
(29) Král, V.; Vašek, P.; Dolenský, B. *Collect. Czech. Chem. Commun.* **2004**, *69*, 1126−1136.
(30) Nemykin, V. N.; Galloni, P.; Floris, B.; Barrett, C. D.; Hadt, R. G.; Subbotin, R. I.; Marrani, A. G.; Zanoni, R.; Loim, N. M. *Dalton Trans.* **2008**, 4233−4246.
(31) Frisch, M. J.; Trucks, G. W.; Schlegel, H. B.; Scuseria, G. E.; Robb, M. A.; Cheeseman, J. R.; Scalmani, G.; Barone, V.; Mennucci, B.; Petersson, G. A.; Nakatsuji, H.; Caricato, M.; Li, X.; Hratchian, H. P.; Izmaylov, A. F.; Bloino, J.; Zheng, G.; Sonnenberg, J. L.; Hada, M.; Ehara, M.; Toyota, K.; Fukuda, R.; Hasegawa, J.; Ishida, M.; Nakajima, T.; Honda, Y.; Kitao, O.; Nakai, H.; Vreven, T.; Montgomery, J. A., Jr.; Peralta, J. E.; Ogliaro, F.; Bearpark, M.; Heyd, J. J.; Brothers, E.; Kudin, K. N.; Staroverov, V. N.; Kobayashi, R.; Normand, J.; Raghavachari, K.; Rendell, A.; Burant, J. C.; Iyengar, S. S.; Tomasi, J.; Cossi, M.; Rega, N.; Millam, J. M.; Klene, M.; Knox, J. E.; Cross, J. B.; Bakken, V.; Adamo, C.; Jaramillo, J.; Gomperts, R.; Stratmann, R. E.; Yazyev, O.; Austin, A. J.; Cammi, R.; Pomelli, C.; Ochterski, J. W.; Martin, R. L.; Morokuma, K.; Zakrzewski, V. G.; Voth, G. A.; Salvador, P.; Dannenberg, J. J.; Dapprich, S.; Daniels, A. D.; Farkas, O.; Foresman, J. B.; Ortiz, J. V.; Cioslowski, J.; Fox, D. J. *Gaussian 09*; Gaussian, Inc.: Wallingford, CT, 2009.
(32) Paolesse, R.; Marini, A.; Nardis, S.; Froiio, A.; Mandoj, F.; Nurco, D. J.; Prodi, L.; Montalti, M.; Smith, K. M. *J. Porphyrins Phthalocyanines* **2003**, *7*, 25−36.
(33) Koszarna, B.; Gryko, D. T. *J. Org. Chem.* **2006**, *71*, 3707−3717.
(34) Steene, E.; Dey, A.; Ghosh, A. *J. Am. Chem. Soc.* **2003**, *125*, 16300−16309.
(35) Ou, Z.; Shao, J.; Zhao, H.; Ohkubo, K.; Wasbotten, I. H.; Fukuzumi, S.; Ghosh, A.; Kadish, K. M. *J. Porphyrins Phthalocyanines* **2004**, *8*, 1236−1247.
(36) Brückner, C.; Brinas, R. P.; Bauer, J. A. K. *Inorg. Chem.* **2003**, *42*, 4495−4497.
(37) Luobeznova, I.; Simkhovich, L.; Goldberg, I.; Gross, Z. *Eur. J. Inorg. Chem.* **2004**, 1724−1732.
(38) Wasbotten, I. H.; Wondimagegn, T.; Ghosh, A. *J. Am. Chem. Soc.* **2002**, *124*, 8104−8116.
(39) Alemayehu, A. B.; Gonzalez, E.; Hansen, L. K.; Ghosh, A. *Inorg. Chem.* **2009**, *48*, 7794−7799.
(40) Alemayehu, A.; Conradie, M. M.; Ghosh, A. *J. Porphyrins Phthalocyanines* **2012**, *16*, 695−704.
(41) Nemykin, V. N.; Rohde, G. T.; Barrett, C. D.; Hadt, R. G.; Sabin, J. R.; Reina, G.; Galloni, P.; Floris, B. *Inorg. Chem.* **2010**, *49*, 7497−7509.
(42) Pierloot, K.; Zhao, H.; Vancoillie, S. *Inorg. Chem.* **2010**, *49*, 10316−10329.
(43) Alemayehu, A. B.; Conradie, J.; Ghosh, A. *Eur. J. Inorg. Chem.* **2011**, 1857−1864.
(44) Thomas, K. E.; Alemayehu, A. B.; Conradie, J.; Beavers, C. M.; Ghosh, A. *Acc. Chem. Res.* **2012**, *45*, 1203−1214.
(45) Vecchi, A.; Erickson, N. R.; Sabin, J. R.; Floris, B.; Conte, V.; Venanzi, M.; Galloni, P.; Nemykin, V. N. *Chem. - Eur. J.* **2015**, *21*, 269−279.
(46) Nemykin, V. N.; Hadt, R. G. *J. Phys. Chem. A* **2010**, *114*, 12062−12066.
(47) Zhang, L.; Qi, D.; Zhang, Y.; Bian, Y.; Jiang, J. *J. Mol. Graphics Modell.* **2011**, *29*, 717−725.
(48) Canard, G.; Gao, D.; D'Aléo, A.; Giorgi, M.; Dang, F.-X.; Balaban, T. S. *Chem. - Eur. J.* **2015**, *21*, 7760−7771.
(49) Paolesse, R.; Licoccia, S.; Bandoli, G.; Dolmella, A.; Boschi, T. *Inorg. Chem.* **1994**, *33*, 1171−1176.
(50) Huang, S.; Fang, Y.; Lü, A.; Lu, G.; Ou, Z.; Kadish, K. M. *J. Porphyrins Phthalocyanines* **2012**, *16*, 958−967.
(51) Nardis, S.; Pomarico, G.; Fronczek, F. R.; Vicente, M. G. H; Paolesse, R. *Tetrahedron Lett.* **2007**, *48*, 8643−8646.
(52) Pomarico, G.; Xiao, X.; Nardis, S.; Paolesse, R.; Fronczek, F. R.; Smith, K. M.; Fang, Y.; Ou, Z.; Kadish, K. M. *Inorg. Chem.* **2010**, *49*, 5766−5774.
(53) Wojaczyński, J.; Duszak, M.; Latos-Grażyński, L. *Tetrahedron* **2013**, *69*, 10445−10449.
(54) Balazs, Y. S.; Saltsman, I.; Mahammed, A.; Tkachenko, E.; Golubkov, G.; Levine, J.; Gross, Z. *Magn. Reson. Chem.* **2004**, *42*, 624−635.
(55) Tardieux, C.; Gros, C. P.; Guilard, R. *J. Heterocycl. Chem.* **1998**, *35*, 965−970.
(56) Paolesse, R.; Sagone, F.; Macagnano, A.; Boschi, T.; Prodi, L.; Montalti, M.; Zaccheroni, N.; Bolletta, F.; Smith, K. M. *J. Porphyrins Phthalocyanines* **1999**, *3*, 364−370.
(57) Nardis, S.; Mandoj, F.; Paolesse, R.; Fronczek, F. R.; Smith, K. M.; Prodi, L.; Montalti, M.; Battistini, G. *Eur. J. Inorg. Chem.* **2007**, 2345−2352.
(58) Kadish, K. M.; Adamian, V. A.; Van-Caemelbecke, E.; Gueletii, E.; Will, S.; Erben, C.; Vogel, E. *J. Am. Chem. Soc.* **1998**, *120*, 11986−11993.
(59) Stefanelli, M.; Mandoj, F.; Mastroianni, M.; Nardis, S.; Mohite, P.; Fronczek, F. R.; Smith, K. M.; Kadish, K. M.; Xiao, X.; Ou, Z.; Chen, P.; Paolesse, R. *Inorg. Chem.* **2011**, *50*, 8281−8292.
(60) Lu, G.; Lin, W.; Fang, Y.; Zhu, W.; Ji, X.; Ou, Z. *J. Porphyrins Phthalocyanines* **2011**, *15*, 1265−1274.
(61) Guilard, R.; Gros, C. P.; Barbe, J.-M.; Espinosa, E.; Jerome, F.; Tabard, A.; Latour, J.-M.; Shao, J.; Ou, Z.; Kadish, K. M. *Inorg. Chem.* **2004**, *43*, 7441−7455.
(62) Barbe, J.-M.; Habermeyer, B.; Khoury, T.; Gros, C. P.; Richard, P.; Chen, P.; Kadish, K. M. *Inorg. Chem.* **2010**, *49*, 8929−8940.
(63) Fang, Y.; Mandoj, F.; Zeng, L.; Pudi, R.; Stefanelli, M.; Paolesse, R.; Kadish, K. M. *J. Porphyrins Phthalocyanines* **2015**, *19*, 388−397.
(64) Rohde, G. T.; Sabin, J. R.; Barrett, C. D.; Nemykin, V. N. *New J. Chem.* **2011**, *35*, 1440−1448.
(65) Adamian, V. A.; D'Souza, F.; Licoccia, S.; Di Vona, M. L.; Tassoni, E.; Paolesse, R.; Boschi, T.; Kadish, K. M. *Inorg. Chem.* **1995**, *34*, 532−540.
(66) Li, B.; Ou, Z.; Meng, D.; Tang, J.; Fang, Y.; Liu, R.; Kadish, K. M. *J. Inorg. Biochem.* **2014**, *136*, 130−139.
(67) Kadish, K. M.; Koh, W.; Tagliatesta, P.; Sazou, D.; Paolesse, R.; Licoccia, S.; Boschi, T. *Inorg. Chem.* **1992**, *31*, 2305−2313.

DOI: 10.1021/acs.inorgchem.5b01575
Inorg. Chem. 2015, 54, 10256−10268